APPLICATION OF A CFD AND PRESCRIBED WAKE MODEL TO HIGH ADVANCE RATIO WIND TUNNEL TEST VALIDATION

Masahiko Sugiura, Japan Aerospace Exploration Agency, Tokyo, Japan
Yasutada Tanabe, Japan Aerospace Exploration Agency, Tokyo, Japan
Hideaki Sugawara, Ryoyu Systems, Nagoya, Japan
Inderjit Chopra, University of Maryland, College Park, USA

Abstract

High speed rotorcraft such as compound, co-axial helicopter and tilt-rotor has been proposed to overcome the flight speed limit of a conventional helicopter. As the design of this high speed rotorcraft proceeds, design tools such as aeromechanics analysis at high advance ratios will be necessary. A hybrid method of CFD and prescribed wake model (HCP) is one of the promising analysis tools. This HCP reduces computational cost by computing only around a blade in CFD, and wake region is computed by prescribed wake model. In this paper, it is validated with the high advance ratio wind tunnel test in the University of Maryland in terms of airload. As a result, an existing HCP shows reasonable results compared with the test data and the comprehensive analysis code UMARC. In addition to that, HCP captures the flow separation from the trailing edge around the blade root area by virtue of using CFD.

1. INTRODUCTION

Recently, high speed rotorcraft such as compound, co-axial helicopter and tilt-rotor has been proposed to overcome the flight speed limit of a conventional helicopter. From this technical background, the conceptual study of high speed rotorcraft by Japan Aerospace Exploration Agency's (JAXA's) group proposed a compound helicopter concept for high speed EMS (Emergency Medical Service) [1]. As the design of this high speed rotorcraft proceeds, design tools such as aeromechanics analysis at high advance ratios will be necessary. In terms of the rotor aeromechanics phenomena in high advance ratio, its fundamental behaviours were revealed by wind tunnel tests and numerical simulations [2-29].

Harris summarized the past researches of high advance ratio rotor in 2008 [2]. Then, Bowen-Davies introduced the recent NASA and UMD (University of Maryland) research activities [3]. Those activities are briefly summarized as follows; from 1930s to 1960s, high advance ratio rotor tests were conducted four times. Firstly, the Pitcairn PCA-2 Autogiro [4] was tested in the NACA full scale wind tunnel, reaching an advance ratio of 0.7. Secondarily, a 15 ft diameter teetering rotor was tested in the Langley full-scale tunnel up to an advance ratio of 1.45 [5]. Then, a H-34 [6] articulated rotor and a UH-1D [7] teetering rotor were also tested to high advance ratios in the NASA 40 by 80 foot wind tunnel. Performance data and blade motions from these experiments have been used to evaluate analyses by several researchers [8-10], however these experiments lacked detailed information about the rotor characteristics, and also, the test data were limited in both quality and extent as needed for the validation of modern, high-fidelity codes.

Recently, the full-scale UH-60A rotor was tested at the U. S. National Full-Scale Aerodynamics Complex (NFAC) at NASA Ames in 2011 [11]. The slowed rotor portion of this test was conducted to provide a comprehensive set of data from which to learn about high advance ratio aeromechanics as well as providing an opportunity to validate existing analysis capability. Datta, Yeo and Norman [12] provided a systematic evaluation of the results as well as a fundamental explanation of the reverse flow physics. There have been several papers dealing with correlation of comprehensive analyses to the UH-60A full-scale data [13-24].

On the other hand, at the University of Maryland, Berry and Chopra [25-27] have carried out tests on twisted and untwisted 4-bladed, Mach-scaled, articulated model rotors in the Glenn L. Martin wind tunnel and achieved an advance ratio of 1.2 from 2011 to 2013 (Fig. 5). More recently, Berry and Chopra have further extended the advance ratio envelope to about 1.6 in two separate wind tunnel entries in 2014 [28, 29]. Using those test data, Bowen-Davies [3, 23] investigated both the earlier and the more recent results with UMARC (University of Maryland Advanced Rotorcraft Code) [30]. The prediction of thrust, including thrust reversal, is satisfactory up to 1.2 advance ratio. The test provides a unique comparison of model-scale data to the full scale UH-60A tests to investigate the role played by blade twist as well as scaling effects and to compare the behavior at thrust reversal. The 2014 Maryland data is the focus of this paper.

Through these research trends, CFD and comprehensive analysis tools were mainly utilized to validate with test data thus far in terms of high advance ratio rotor analysis. CFD is suited for understanding of detailed fluid phenomena. On the other hand, comprehensive analysis tools are useful for design since a number of parameters can be handled by their high computational efficiency. Among analysis tools, a hybrid method of CFD and prescribed wake model (HCP) is between CFD and the comprehensive analysis tools with respect to computational accuracy and cost. In this HCP, the region around a blade is numerically simulated by CFD and the far wake region is represented by a prescribed wake model. HCP can only be applied to an isolated rotor, but its computational cost is one-fifteenth of full CFD by using the prescribed wake model as a substitute for background CFD grids. Thus far, JAXA has been improving progressively this HCP, which was proposed by Yang et. al. [31] in terms of computational accuracy by transferring CFD information to the prescribed wake model [32, 33]. The objective of this paper is to evaluate the capability of HCP to predict the airloads at high advance ratios.

2. NUMERICAL METHODS

The baseline CFD code is a structured grid flow solver, <rFlow3D>, which has been systematically developed at JAXA for rotorcraft applications [34]. The rFlow3D is a highly versatile CFD code that can numerically simulate flows around rotorcraft in a wide range of Reynolds and Mach numbers, including rotor trim analysis with elastic blade deformations. As a prescribed wake model, modified Beddoes' model is employed in this study, as it was shown in the previous study that modified Beddoes' model agrees well with test data among available prescribed wake models [32].

2.1. CFD

The governing equation of CFD is three dimensional compressible Navier-Stokes equations:

$$(1)\qquad \frac{\partial}{\partial t}\int_{V(t)}\mathbf{U}\,\mathrm{d}V+\int_{S(t)}(\mathbf{F}^{i}-\mathbf{F}^{V})\cdot\mathbf{n}\mathrm{d}S=0$$

where $\mathbf{U}$ is the conservative flow variable vector, $\mathbf{F}^{i}$ and $\mathbf{F}^{V}$ are inviscid and viscous flux vector, respectively. V(t) is the time-varying cell volume and S(t) is the time-varying cell boundary. $\mathbf{n}$ is the unit normal vector to the cell surface. The flow field is assumed as a laminar flow, since the tip Reynolds number shown in Table 1 in the section 3 is approximately one million. Components of $\mathbf{U}$, $\mathbf{F}^{i}$ and $\mathbf{F}^{V}$ are as follows:

$$(2)\qquad \mathbf{U}=\begin{pmatrix}\rho\\ \rho\mathbf{v}\\ \rho e\end{pmatrix},\ \ \mathbf{F}^{i}\cdot\mathbf{n}=\begin{pmatrix}(\mathbf{v}-\dot{\mathbf{x}})\cdot\mathbf{n}\rho\\ (\mathbf{v}-\dot{\mathbf{x}})\cdot\mathbf{n}\rho\mathbf{v}+p\mathbf{n}\\ (\mathbf{v}-\dot{\mathbf{x}})\cdot\mathbf{n}\rho e+p\mathbf{v}\cdot\mathbf{n}\end{pmatrix},$$

$$\mathbf{F}^{V}\cdot\mathbf{n}=\begin{pmatrix}0\\ \boldsymbol{\tau}\cdot\mathbf{n}\\ (\boldsymbol{\tau}\cdot\mathbf{v}-\mathbf{q})\cdot\mathbf{n}\end{pmatrix}$$

v is the velocity vector for x, y, z directions, $\dot{\mathbf{x}}$ is the velocity vector of moving cell boundary, ρ is air density, *p* is pressure, and *e* is total energy.

Finite volume method and moving overlapped grid method are used in this numerical solution. mSLAU (modified Simple Low-dissipation AUSM) [35] which is modified for applying all-speed SLAU scheme to moving overlapped grid method is used for numerical velocity, and fourth spatial precision FCMT (Fourth-order Compact MUSCL TVD) scheme [36] is used for reconstruction of physical values. For time integration, fourth-order Runge-Kutta method is used in background orthogonal grid, and dual-time stepping method [37] is used in blade and fuselage grids to construct unsteady implicit method. LU-SGS/DP-LUR is used for simulated time integration. Tri-Linear interpolation method is used for exchange of values among grids.

2.2. Prescribed Wake Model

There are several blade tip vortex models. In this study, Vatistas n=2 model [38] is employed since it agrees well with experiments. Figure 1 shows Vatistas model with Lamb-Oseen and Rankine models. Blade tip vortex models which include dissipation effect [40] accurately evaluate vortex even if the time is long until blade interacts with vortex. The time evolution of vortex core radius r_c is given as follows:

$$(3)\qquad r_c(t)=\sqrt{r_{c0}^2+4\alpha\delta\upsilon t}$$

where *t* is time, r_{c0} is an initial value of vortex core

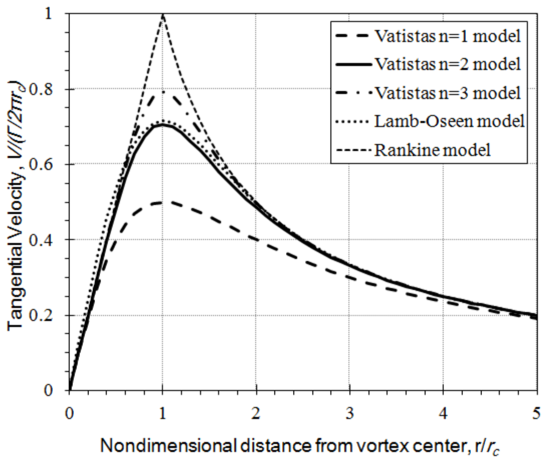

Fig. 1. Comparison of vortex wake model's tangential velocity [39].

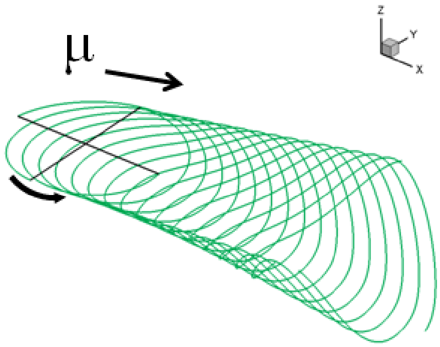

Fig. 2. Vortex wake trajectory of modified Beddoes's model.

radius, which is set as twenty percent of blade cord length in this study. α=1.25643, which is called Oseen parameter. υ is dynamic viscosity coefficient, and δ is called effective diffusion constant or eddy viscosity coefficient which is determined by vortex Reynolds number. Induced velocity by vortices are calculated based on the Biot-Savrt law.

Blade tip vortex moves downward gradually by rotor downwash, and the geometry of blade tip vortex has inclination to the rotor plane (Fig. 2). There are some models in prescribed wake model to describe this three dimensional vortex geometry: rigid model, Beddoes's model [41], and modified Beddoes's model [42]. Rigid model describes blade tip vortex as cylindrical spiral, Beddoes's model includes symmetrical roll-up of blade tip vortex, and modified Beddoes's model reflects asymmetrical roll-up structure of blade tip vortex. Skew angle of blade tip vortex is represented as E=|χ| in both Beddoes's model and modified Beddoes's model. Induced velocity is different among prescribed wake models, however, modified Beddoes's model which considers conservation of momentum and asymmetry of downwash in horizontal direction is explained below since it is most realistic and closest to experiment [32].

In modified Beddoes's model, vortex trajectory projection to x-y plane is assumed as a simple epi-cycloid, and x-y coordinate is expressed as follows:

(4) $$x_v = R\cos\Psi_v + \mu_x \Delta\Psi_v$$
(5) $$y_v = R\sin\Psi_v$$

where x_v and y_v indicate blade tip vortex coordinate. R is radius of rotor, Ψ_v is blade rotation angle when blade tip vortex is generated, $\mu_x = V\cos\alpha_{TPP}/R\Omega$, $\Delta\Psi_v = \Psi_b - \Psi_v$, V is uniform flow velocity, α_{TPP} is rotor plane's angle of attack, Ω is blade rotation angular velocity, Ψ_b is blade rotation angle in computational time. Z coordinate is given as integral of rotor inflow's downward component and downwash v

(6) $$z_v = (1/R\Omega)\int_{\Psi_v}^{\Psi_b}(-V\sin\alpha_{TPP} + v)\,d\Psi$$
$$= \int_{\Psi_v}^{\Psi_b}(-\mu_z + v/R\Omega)\,d\Psi$$
$$= -\mu_z\Delta\Psi_v + \int_{\Psi_v}^{\Psi_b}(v/R\Omega)\,d\Psi$$

where $\mu_z = V\sin\alpha_{TPP}/R\Omega$ and downwash v is defined as follows:

(inside rotor disc)

(7) $$v = v_0(1 + 8E/15\pi + Ex' - 2\mu_x y' - E|y'^3|)$$

(outside rotor disc)

(8) $$v = 2v_0(1 + 8E/15\pi - 2\mu_x y' - E|y'^3|)$$

considering inhomogeneous downwash distribution to the longitudinal and lateral directions. The second term in right-hand side of eq. (6) is integrated by using eqs. (7) and (8). Variables with prime in eqs. (7) and (8) indicate that they are normalized by rotor radius R. v_0 is given as $v_0 = -\lambda_I R\Omega$, assuming uniform downwash inside rotor disc. λ_I is a solution of the following equation:

(9) $$-C_T/2\lambda_I = [(\mu_z + \lambda_I)^2 + \mu_x^2]^{1/2}$$

Wake inclination to the longitudinal direction is expressed as E=|χ| using following skew angle:

(10) $$\chi = \tan^{-1}[\mu_x/-(\mu_z + \lambda_I)]$$

2.3. Hybrid Method of CFD and Prescribe Wake Model (HCP)

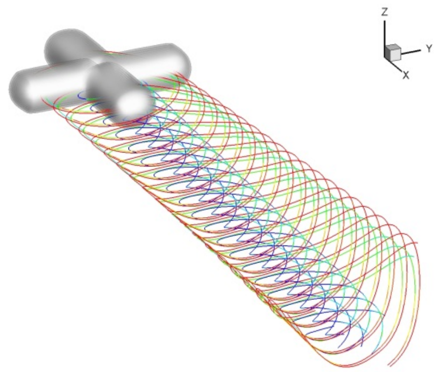

Fig. 3. Configuration of CFD region and prescribed wake model in HCP.

This HCP reduces computational cost by computing only around a blade in CFD, and wake region is computed by prescribed wake model, assuming wake region is potential. Density, momentum, and energy in CFD are computed by reflecting induced velocity of blade tip vortex which is calculated by prescribed wake model. In particular, induced velocity of prescribed wake model is added to three outer layer grids in CFD to satisfy mass conservation law since the effect of compression is little in the area far from the blade [31]. Configuration of CFD computational grids and prescribed wake model is shown in Fig. 3.

At the interface of CFD and prescribed wake model, variables of flow field are calculated by the following equations [31]:

$$\begin{pmatrix} u \\ v \\ w \end{pmatrix} = \begin{pmatrix} u_\infty + u_w \\ v_\infty + v_w \\ w_\infty + w_w \end{pmatrix} \tag{11}$$

$$\rho = \left(\frac{a^2}{a_\infty^2}\right)^{\frac{1}{\gamma-1}} \tag{12}$$

$$e = \rho\left[\frac{a^2}{\gamma(\gamma-1)} + \frac{u^2+v^2+w^2}{2}\right] \tag{13}$$

where u, v, w are flow velocity components in x, y, z directions, respectively, a is sound speed, γ is specific heat ratio, ∞ means component of uniform flow, and w means component of wake. Local sound speed is determined from the following energy equation:

$$a^2 = a_\infty^2 + \frac{\gamma-1}{2}\left[V_\infty^2 - (u^2+v^2+w^2)\right] \tag{14}$$

V_∞ is velocity of main stream.

Figure 4 shows the flow chart of HCP computation procedure. Every time trim is set, for example, every 180 deg. azimuth angle in four blades, the following steps are processed; (1) sectional circulation on each azimuth angle is calculated by using CFD information, (2) multi-trailers are generated based on lifting line theory, (3) the circulation of prescribed wake model is scaled to correspond to the thrust coefficient in CFD.

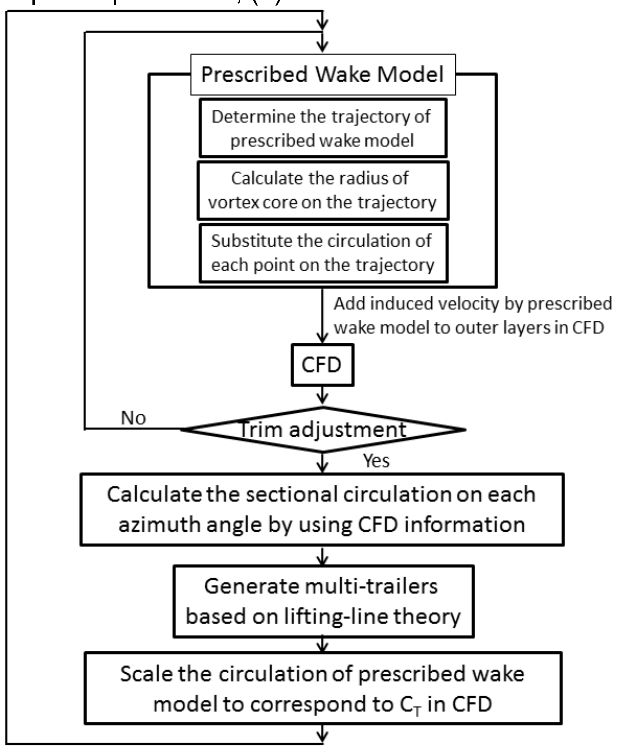

Fig. 4. Flow chart of HCP computation procedure.

2.4. Trim

The rotor pitch angles are adjusted so that the rotor thrust and moments agrees with the target trim rotor values. Trim adjustment renewal has been done after a half revolution of aerodynamic loading is obtained and during the next cycle of CFD calculations, the rotor trim controls are frozen.

The trim adjustment is based on the partial derivatives of the rotor thrust and moments to the rotor controls as the following equations:

$$\begin{bmatrix} \Delta\theta_0 \\ \Delta\theta_c \\ \Delta\theta_s \end{bmatrix} = \begin{bmatrix} \frac{\partial T}{\partial\theta_0} & \frac{\partial T}{\partial\theta_c} & \frac{\partial T}{\partial\theta_s} \\ \frac{\partial Mx}{\partial\theta_0} & \frac{\partial Mx}{\partial\theta_c} & \frac{\partial Mx}{\partial\theta_s} \\ \frac{\partial My}{\partial\theta_0} & \frac{\partial My}{\partial\theta_c} & \frac{\partial My}{\partial\theta_s} \end{bmatrix}^{-1} \begin{bmatrix} \Delta T \\ \Delta \mathrm{Mx} \\ \Delta \mathrm{My} \end{bmatrix} \tag{15}$$

$$\begin{aligned} \Delta T &= T_{TARGET} - \left(T_{CFD} + T_{BET} + T_{BET,0}\right) \\ \Delta Mx &= Mx_{TARGET} - \left(Mx_{CFD} + Mx_{BET} + Mx_{BET,0}\right) \\ \Delta My &= My_{TARGET} - \left(My_{CFD} + My_{BET} + My_{BET,0}\right) \end{aligned} \tag{16}$$

The partial derivatives are numerically obtained based on the simple blade element theory where the inflow is uniform and depending on the target thrust only. To improve the computational stability and convergence, the trim adjustment are added with a relaxation factor multiplied.

3. NUMERICAL CONDITIONS

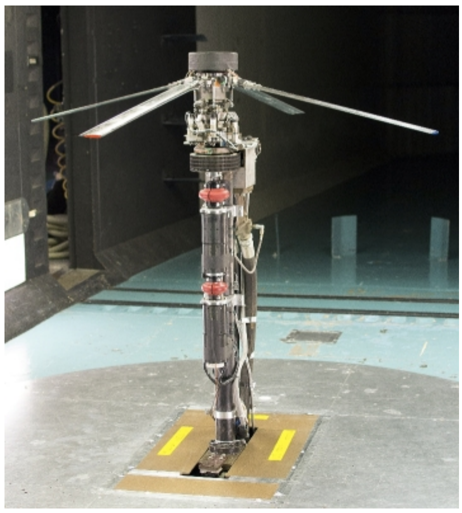

Fig. 5. Rotor test stand installed in the Glenn L. Martin Wind Tunnel [29].

Figure 5 and Table 1 show an overview of the high advance ratio wind tunnel test in UMD [29]. HCP is validated with this wind tunnel test data. Testing was performed on a 1.7 m (5.6 ft) diameter model rotor using a Mach-scale fully articulated rotor test stand. Figure 5 shows the model rotor setup installed in the wind tunnel. The rotor blades were constructed in-house. The blade contained embedded pressure transducers in a chordwise arrangement at a single radial station, 0.3R (Table 2). This station was chosen to investigate the impact of high reverse-flow velocities while maintaining distance from blade root effects. Figure 6 shows a sketch of the size and location of the embedded transducers in the rotor blade airfoil.

Table 1: Rotor properties [29].

Number of blades	4
Radius, m (ft)	0.849 (2.79)
Chord, cm (in)	8.0 (3.15)
Solidity	0.120
Lock No.	5.5
Airfoil section	NACA 0012
100% RPM	2300
Tip speed, m/s (ft/s)	206 (675)
Tip Mach	0.60
Tip Reynolds	1.1×10^{6}
Hinge offset	6.3%
Root cutout	22.3%

Table 2: Non-dimensional chordwise distribution of the 19 blade pressure transducers (0.3R station). Highlighted sensors were not functional for the entire testing program [29].

	Upper surface (x/c)	Lower surface (x/c)
1	0.029	0.029
2	0.076	0.076
3	0.127	0.127
4	0.190	0.190
5	0.317	0.317
6	0.460	0.460
7	0.603	0.603
8	0.730	0.730
9	0.829	0.790
10	-	0.879

Fig. 6. Airfoil cross-section (8.0 cm, 3.15" total chord length) showing chordwise placement of em-bedded pressure transducers [29].

Table 3: μ sweep at a collective pitch angle of 4 deg..

μ	Tip Mach	C_T/σ
0.25	0.18	0.0402
0.41	0.18	0.0346
0.62	0.18	0.0236
0.72	0.25	0.0200
0.83	0.18	0.0113
1.03	0.18	0.0042
1.20	0.15	-0.0204

In the wind tunnel test, collective sweeps were performed at several advance ratios from 0 to 1.5. Among these data, several advance ratio cases with constant pitch angle are selected as a first step in this study to confirm the advance ratio effect on HCP (Table 3). In these conditions, the shaft angle is zero degree.

4. NUMERICAL RESULTS

4.1. Normal Force

Normal force calculated by HCP is compared with the measured data as well with the prediction from comprehensive analysis UMARC [30] in Fig. 6. Normal force of the experiment is estimated by trapezoidal integration using the pressure data and the distance between the pressure sensors. At all the advance ratios, HCP generally shows good agreement with UMARC. Both prediction codes provide satisfactory correlation with test data. However, test data shows negative normal force at very low azimuthal angles. Note the effect of hub is not included in the analyses (Figs. 3 and 5). Thus, only the predicted results show significant blade vortex interactions on the advancing side at the advance ratio of 0.25. At the advance ratios higher

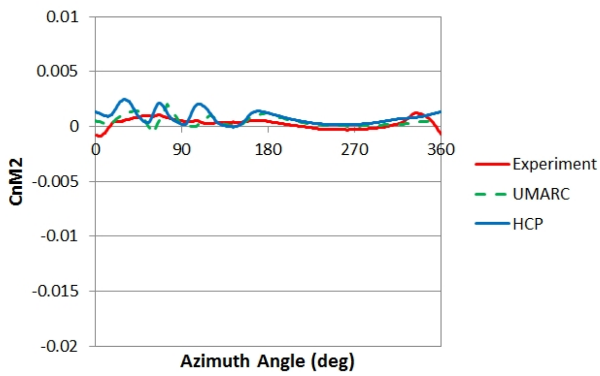

$\mu = 0.25$

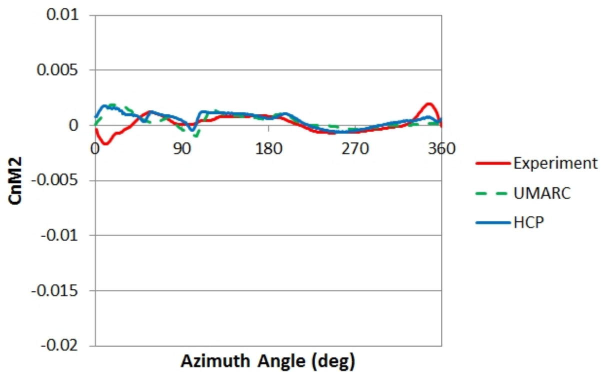

$\mu = 0.41$

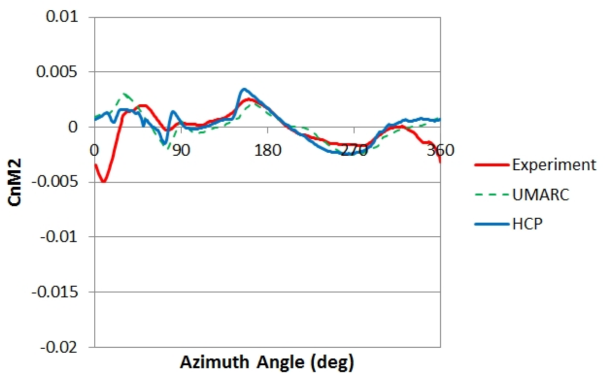

$\mu = 0.62$

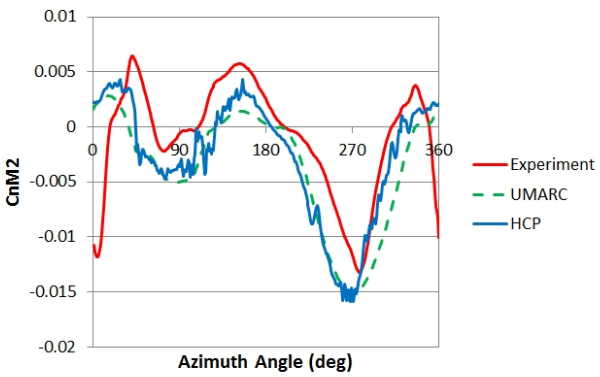

$\mu = 1.20$

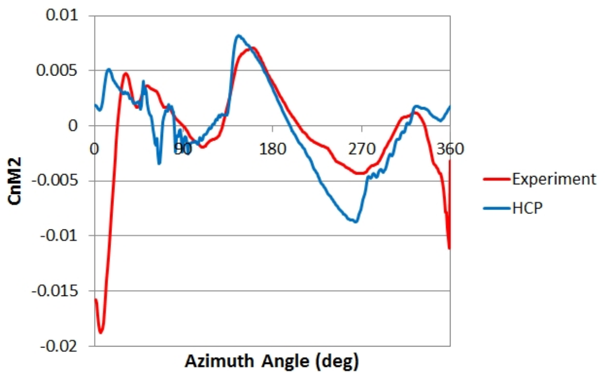

$\mu = 0.72$

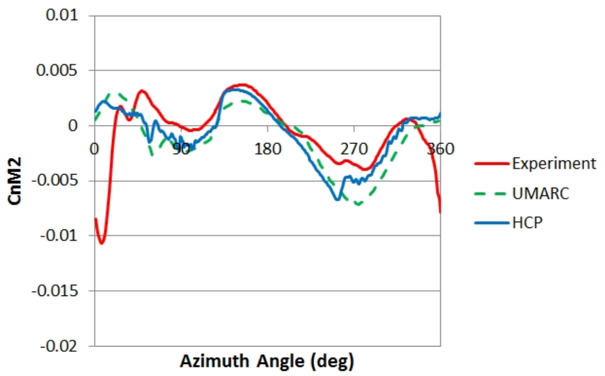

$\mu = 0.83$

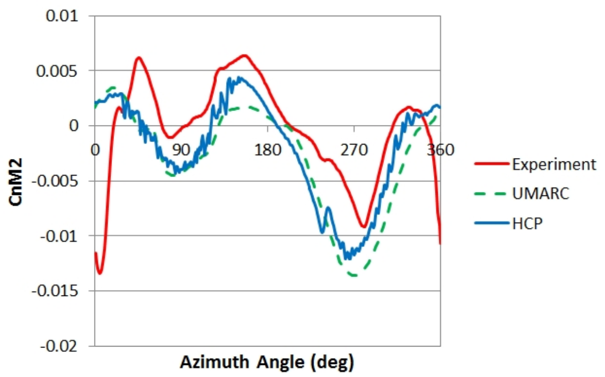

$\mu = 1.03$

Fig. 6. Comparisons of normal forces among experiment, UMARC and HCP.

than 0.72, HCP have high oscillations on the normal force. The cause of these oscillations will be discussed in the following subsections. At the advance ratios of 1.03 and 1.20, test data shows larger normal force values compared with both prediction codes.

4.2. Flow Separation from Trailing Edge

In this subsection, the cause of high frequency oscillations in normal force of HCP is investigated. Figure 7 shows normal force distributions of HCP. The blade 30% radius spanwise location is shown by black solid circle. From this figure, the oscillation of normal force is clearly seen in the blade root area at the advance ratios higher than 0.72 (black dashed circle area in Fig. 7). The flow filed is actually turbulent in the blade root area at an azimuth angle of 90 deg. as shown in the red circle in Fig. 8. The blade surface is contoured by air pressure and iso-vorticity surface is also described by blue colour. The blade root area is enlarged in Fig. 9. Flow separation from the trailing edge occurs at the advance ratios higher than 0.62. Flow separation region spread toward the leading edge as the advance ratio increases. From this figure, the oscillation of normal force is supposed to be generated by the turbulent flow in the rear of the

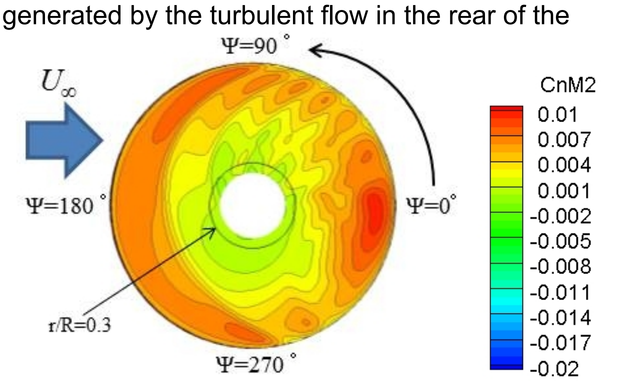

$\mu = 0.25$

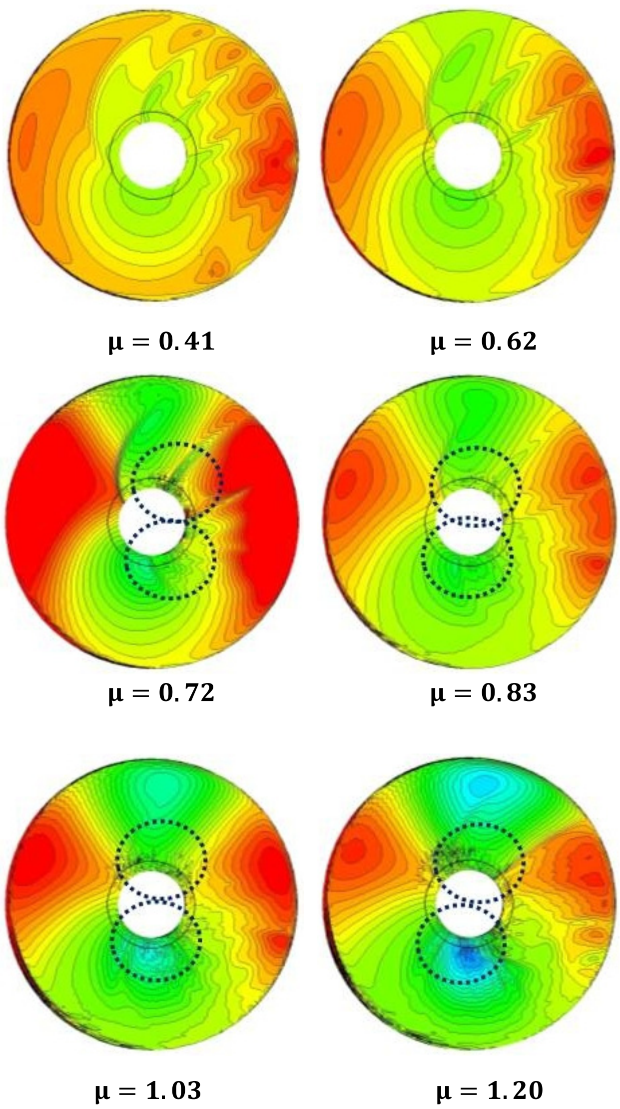

Fig. 7. Normal force distributions of HCP.

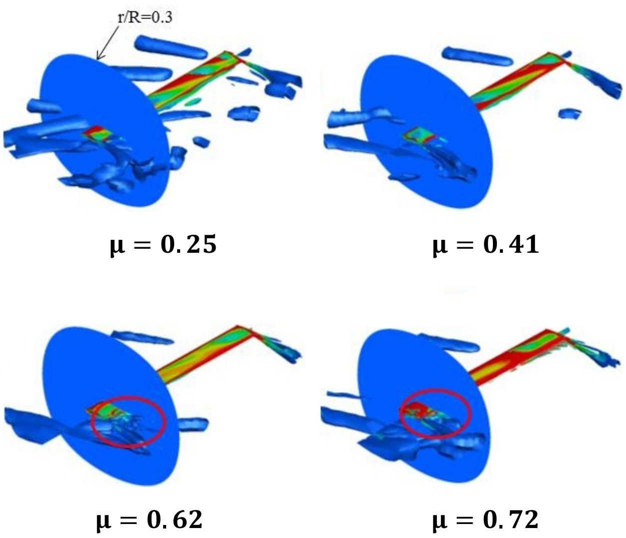

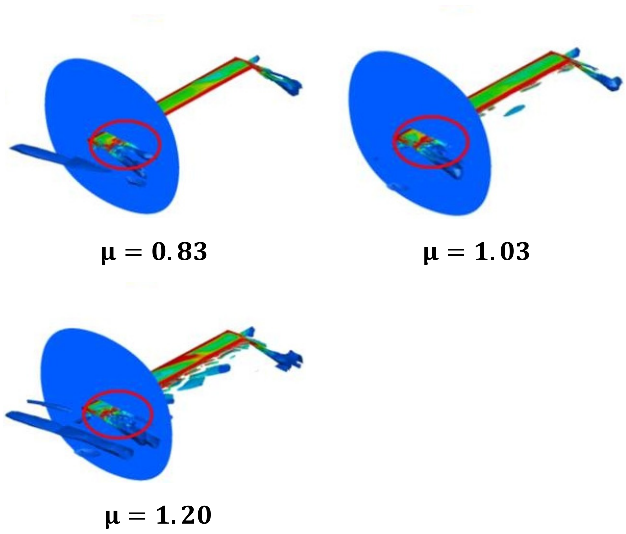

Fig. 8. Flow filed of HCP at an azimuth angle of 90 deg..

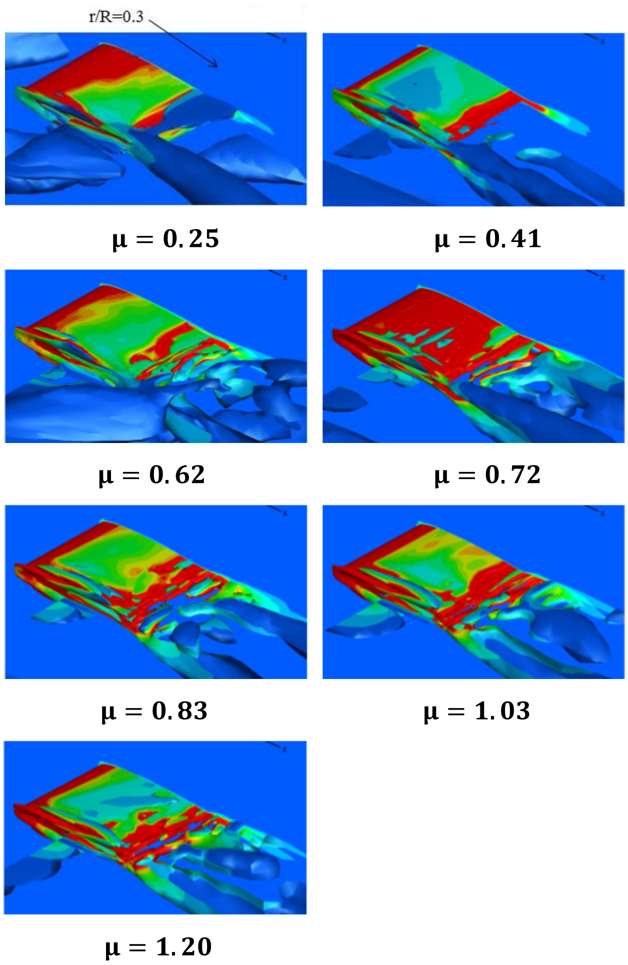

Fig. 9. Flow field of HCP at an azimuth angle of 90 deg. (the blade root area is enlarged).

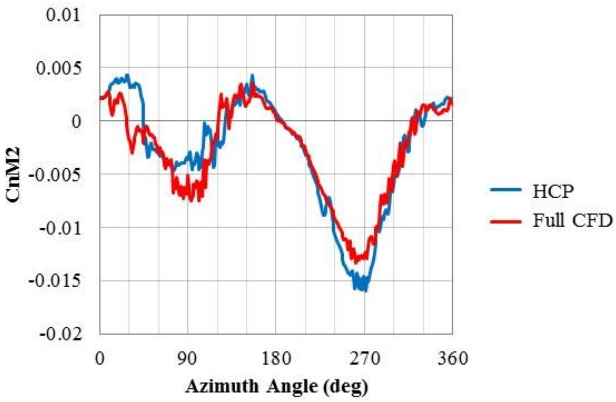

Fig. 10. Comparison of sectional normal forces between HCP and full CFD (at r/R=0.30, μ =1.20).

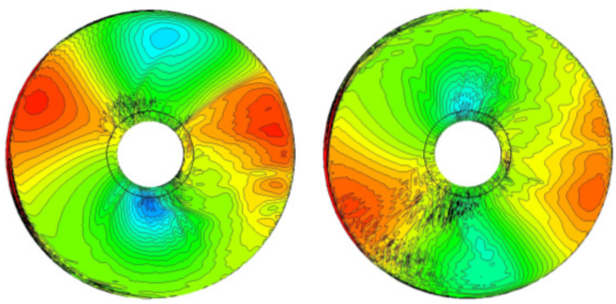

HCP Full CFD

Fig. 11. Comparisons of normal force distributions between HCP and full CFD.

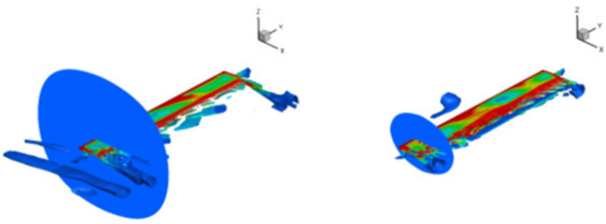

HCP Full CFD

Fig. 12. Flow filed at an azimuth angle of 90 deg..

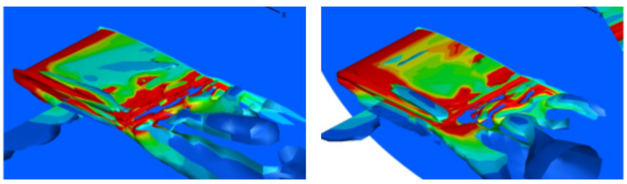

HCP Full CFD

Fig. 13. Flow field at an azimuth angle of 90 deg. (the blade root area is enlarged).

blade especially at the advance ratios higher than 0.72. The reason that the oscillations are not found in test data is supposed to be due to data filtering process. And the cause that UMARC does not generate the oscillations is supposed to be originated in its two dimensional nature of lifting line.

4.3. Comparison with full CFD

In this subsection, HCP is validated by comparing with full CFD. Full CFD means all the space including the far wake field is covered with grids and computed by CFD. Figure 10 shows sectional normal forces at 30% radius spanwise location. There is a slight difference in normal force between them, but the similar high frequency oscillations are generated. Figure 11 shows both distributions have high frequency oscillation regions at the blade root area, though there is a phase difference in high and low normal force regions. Figure 12 is the images of flow filed at an azimuth angle of 90 deg. and the blade root area is enlarged in Fig. 13. From these figures, we can see both simulations show quite good agreement. Therefore, it can be said that HCP has almost the same computational accuracy in predicting normal force and flow filed around a blade at high advance ratio.

5. CONCLUDING REMARKS

The hybrid method of CFD and prescribed wake model is validated with the wind tunnel test data of UMD from low to high advance ratio. As a result, an existing HCP shows reasonable results compared with the test data and the comprehensive analysis. In addition to that, HCP captures the flow separation from the trailing edge around the blade root area by virtue of using CFD. The blade vibration phenomena in the high advance ratio observed in the wind tunnel test will be validated in the near future by using CFD/CSD coupling.

ACKNOWLEGEMENTS

The authors would like to thank Dr. Graham Bowen-Davies who provided us UMARC data, as well as the support from Mr. Ben Berry, for sharing the UMD wind tunnel test data.

REFERENCES

[1] Tanabe, Y., Aoyama, T., Kobiki, N., Sugiura, M., Miyashita, R., Sunada, S., Kawachi, K. and Nagao, M. A Conceptual Study of High Speed Rotorcraft. The 40th European Rotorcraft Forum, Southampton, England, 2014.

[2] Harris, F. D. Rotor Performance at High Advance Ratio; Theory versus Test. NASA CR 2008-215370, 2008.

[3] Bowen-Davies, G. and Chopra, I. Aero-mechanics of a Slowed Rotor. The American Institute of Aeronautics and Astronautics Science

and Technology Forum, Kissimmee, FL, USA, 2015.

[4] Wheatley, J. B. and Hood, M. L. Full-Scale Wind-Tunnel Tests of a PCA-2 Autogiro Rotor. NACA Report No. 515, 1935.

[5] Jenkins, J.L., Jr. Wind Tunnel Investigation of a Lifting Rotor Operating at Tip-Speed Ratios from 0.65 to 1.45. NASA TN-D-2628, 1965.

[6] McCloud, J. L., Biggers, J. C. and Stroub, R. H. Ratios and Advance Ratios and Advancing Tip Mach Numbers. NASA TN D-4632, 1968.

[7] Charles, B. D. and Tanner, W. H. Wind Tunnel Investigation of Semirigid Full-Scale Rotors Operating at High Advance Ratios. United States Army Aviation Material Laboratories TR 69-2, 1969.

[8] Yeo, H. and Johnson, W. Optimum Design of a Compound Helicopter. Journal of Aircraft, Vol. 46, No. 4, 2009.

[9] Floros, M. and Johnson, W. Performance analysis of the Slowed-Rotor Compound Helicopter Configuration. Journal of the American Helicopter Society, Vol. 54, 2009.

[10] Ormiston, R. Rotor Aerodynamic Characteristics at High Advance Ratio Relevant to Compound Rotorcraft. The American Helicopter Society Future Vertical Lift Aircraft Design Conference, San Francisco, CA, USA, 2012.

[11] Norman, T. R., Shinoda, P. M., Peterson, R. L. and Datta, A. Full-scale Wind Tunnel Test of the UH-60A Airloads Rotor. The American Helicopter Society 67th Annual Forum, Virginia Beach, VA, USA, 2011.

[12] Datta, A., Yeo, H. and Norman, T. Experimental Investigation and Fundamental Understanding of a Slowed UH-60A Rotor at High Advance Ratios. The American Helicopter Society 67th Annual Forum, Virginia Beach, VA, USA, 2011.

[13] Kottapalli, S. Performance and Loads Correlation of A UH-60A Slowed Rotor at High Advance Ratios. The American Helicopter Society Future Vertical Lift Aircraft Design Conference, San Francisco, CA, USA, 2012.

[14] Yeo, H. Investigation of UH-60A Rotor Performance and Loads at High Advance Ratios. Journal of Aircraft, Vol. 50, No. 2, 2013.

[15] Johnson, W. Technology Drivers in the Development of CAMRAD II. The American Helicopter Society Aeromechanics Specialists Meeting, San Francisco, CA, USA, 1994.

[16] Ormiston. R. Rotor Aerodynamic Characteristics at High Advance Ratios Relevant to Compound Rotorcraft. The American Helicopter Society Future Vertical Lift Aircraft Design Conference, San Francisco, CA, USA, 2012.

[17] Potsdam, M., Datta, A. and Jayaraman, B. Computational Investigation and Fundamental Understanding of A Slowed UH-60A Rotor at High Advance Ratios. The American Helicopter Society 68th Annual Forum, Fort Worth, TX, USA, 2012.

[18] Potsdam, M., Yeo, H. and Ormiston, R. Performance and Loads Predictions of A Slowed UH-60A Rotor at High Advance Ratios. The 39th European Rotorcraft Forum, Moscow, Russia, 2013.

[19] Lee-Rausch, E. and Biedron, R., FUN3D Airload Predictions for the Full-Scale UH-60A Airloads Rotor in a Wind Tunnel. The American Helicopter Society 69th Annual Forum, Phoenix, AZ, USA, 2013.

[20] Biedron, R. and Lee-Rausch, E. Blade Displacement Predictions for the Full-Scale UH-60A Airloads Rotor. The American Helicopter Society 70th Annual Forum, Montreal, Canada, 2014.

[21] Bowen-Davies, G. and Chopra, I. Investigation of the UH-60A Slowed Rotor Wind Tunnel Tests using UMARC. The American Helicopter Society 69th Annual Forum, Phoenix, AZ, USA, 2013.

[22] Bowen-Davies, G. and Chopra, I. Correlation of the UH-60A Slowed Rotor Wind Tunnel Tests Using UMARC. The American Helicopter Society 69th Annual Forum, Phoenix, AZ, USA, 2013.

[23] Bowen-Davies, G. and Chopra, I. Validation of Rotor Performance and Loads at High Advance Ratio. The Fifth Decennial American Helicopter Society Aeromechanics Specialists' Conference, San Francisco, CA, USA, 2014.

[24] Bowen-Davies, G. and Chopra, I. Performance and Loads Correlation of the UH-60 Rotor at High Advance Ratios. The 40th European Rotorcraft Forum, Southampton, England, 2014.

[25] Berry, B. and Chopra, I. Wind Tunnel Testing for Performance and Vibratory Loads of a Variable-Speed Mach-Scale Rotor. The American Helicopter Society 67th Annual Forum, Virginia Beach, VA, USA, 2011.

[26] Berry, B., and Chopra, I. Performance and Vibratory Load Measurements of a Slowed-Rotor at High Advance Ratios. The American Helicopter Society 68th Annual Forum, Fort Worth, TX, USA, 2012.

[27] Berry, B. and Chopra, I. High-Advance Ratio Wind Tunnel Testing of Two Mach-Scale Rotor Geometries. The American Helicopter Society 69th Annual Forum, Phoenix, AZ, USA, 2013.

[28] Berry, B. and Chopra, I. High-Advance Ratio Wind Tunnel Testing of a Model Rotor with Pressure Measurements. The Fifth Decennial American

Helicopter Society Aeromechanics Specialists' Conference, San Francisco, CA, USA, 2014.

[29] Berry, B. and Chopra, I. Slowed Rotor Wind Tunnel Testing of An Instrumented Rotor at High Advance Ratio. The 40th European Rotorcraft Forum, Southampton, England, 2014.

[30] Chopra, I. and Bir, G, University of Maryland Advanced Code: UMARC. The American Helicopter Society Aeromechanics Specialists Conference, San Francisco, CA, USA, 1994.

[31] Yang, Z., Sankar, L. N. Smith, M. J. and Bauchau, O. Recent Improvements to a Hybrid Method for Rotors in Forward Flight. Journal of Aircraft, Vol.39, No.5, 2002.

[32] Sugiura, M., Tanabe, Y., and Sugawara, H. Development of a Hybrid Method of CFD and Prescribed Wake Model for Helicopter BVI Noise Prediction. Trans. Japan Soc. Aero. Space Sci., Vol.56, No.6, 2013.

[33] Sugiura, M., Tanabe, Y., and Sugawara, H. Development of a Hybrid Method of CFD and Prescribed Wake Model for Helicopter BVI Noise Prediction. The American Helicopter Society 69th Annual Forum, Phoenix, AZ, USA, 2013.

[34] Tanabe, Y., Saito, S., and Sugawara, H. Evaluation of Rotor Noise Reduction by Active Devices Using a CFD/CSD Coupling Analysis Tool Chain. The 1st Asian Australian Rotorcraft Forum and Exhibition 2012, Busan, Korea, 2012.

[35] Tanabe, Y. and Saito, S. Significance of All-Speed Scheme in Application to Rotorcraft CFD Simulation. The 3rd International Basic Research Conference on Rotorcraft Technology, Nanjing, China, 2009.

[36] Yamamoto, S. and Daiguji, H. High-Order-Accurate Upwind Schemes for Solving the Compressible Euler and Navier-Stokes Equations. Computers & Fluids ,Vol.22, No2/3, 1993.

[37] Zhang, L. P. and Wang, Z. J. A block LU-SGS implicit dual time-stepping algorithm for hybrid dynamic meshes. Computers & Fluids, Vol.33, 2004.

[38] Vatistas, G. H., Kozel, V. and Mih, W. C. A Simpler Model for Concentrated Vortices. Experiments in Fluids, Vol.11, 1991.

[39] Leishman, J. G. Principles of Helicopter Aerodynamics (second edition). Cambridge University Press, 2006.

[40] Bhagwat, M. J. and Leishman, J. G. Generalized Viscous Vortex Model for Application to Free-Vortex Wake and Aeroacoustic Calculations. The American Helicopter Society 58th Annual Forum, Montreal, Canada, 2002.

[41] Beddoes, T. S. A Wake Model for High Resolution Airloads. The 2nd International Conference on Basic Rotorcraft Research, Research Triangle Park, NC, USA, 1985.

[42] van der Wall, B. G. The Effect of HHC on the Vortex Convection in the Wake of a Helicopter Rotor. Aerospace Science and Technology, Vol. 4, 2000.